JOURNAL OF MATERIALS SCIENCE 29 (1994) 2436–2444

Synthesis of amorphous and metastable $Ti_{40}Al_{60}$ alloys by mechanical alloying of elemental powders

W. GUO, A. IASONNA, M. MAGINI, S. MARTELLI, F. PADELLA
Amorphous Materials Project, E.N.E.A. Casaccia Dept. INN-NUMA, C.P. 2400 A.D., I-00100 Rome, Italy

$Ti_{40}Al_{60}$ amorphous and metastable alloys have been prepared by mechanical alloying (MA), under controlled milling conditions in a planetary mill. Three different quantities of kinetic energy at the collision instant have been achieved by using balls of different size, $\phi_b = 5$, 8 and 12 mm, keeping constant all other device parameters. Assuming the collision between the balls and the vial walls to be inelastic, during the early stage of alloying, the amount of energy transferred to the trapped powder could be estimated. The experimental results show that the milling with balls of diameter $\phi_b = 5$ or 8 mm leads to a solid-state amorphization of the $Ti_{40}Al_{60}$ mixture, through the attainment of a supersaturated solid solution of aluminium into α-titanium. Otherwise, the milling causes the nucleation of the A1-fcc disordered form of the TiAl intermetallic compound. The end products of MA-induced solid-state reaction (SSR) have been ascribed to the different temperature reached by the powder during each collision and to the reaction time scale for the formation of the amorphous phase, δt_a, and for the nucleation of the non-equilibrium intermetallic compound, δt_d. Differential scanning calorimetry has indicated that the crystallization of amorphous samples follows a two-step reaction. At a temperature $T_c \approx 400\,°C$, the amorphous phase crystallizes into the A1-fcc. TiAl phase having a measured heat of crystallization of 6.2 kJ $(g\,at)^{-1}$. Upon further heating, the system undergoes $A1 \rightarrow L1_0$ reordering transition with an enthalpy release of about 3.2 kJ $(g\,at)^{-1}$.

1. Introduction

The titanium aluminide intermetallic alloys α_2-(Ti_3Al) and γ-(TiAl) have long been recognized as potentially useful structural materials because they have excellent high-temperature capabilities as a result of their strong ordered bonding and resistance to dislocation motion. However, the localized atomic bonding and associated ordering also cause their brittleness and low fracture toughness at room temperature. These shortcomings appear to be, particularly for γ-(TiAl) alloys, the most serious obstacles to their industrial application.

The γ-(TiAl) intermetallic compound is known to have and $L1_0$ tetragonal structure (prototype CuAu) which remains ordered to its melting point and to exist for an Al composition ranging between 48 and 56.5 at % (Fig. 1). In recent years, much effort has been devoted to improve the mechanical properties of the γ-(TiAl) phase, and some recent investigations have been concerned with the possibility of rapid quenching techniques to reduce partially the long-range order of this structure and to increase ductility by reducing planar faults energies. Rapid solidification processing of TiAl alloys has been shown to improve both the hot workability and the low-temperature ductility of the γ-(TiAl) phase [1], but neither amorphous alloys nor a noticeable suppression of ordering could be attained by such a method [1, 2].

Conversely, mechanical alloying (MA), which has become a widely used technique for the formation of amorphous or metastable alloys (see [3] for a recent review), has been already successfully applied to this system and the synthesis of amorphous powder has been attained for the compositional range $Ti_{1-x}Al_x$ ($20 \leqslant x \leqslant 50$ at %) [4, 5].

We have further observed [4], that the limiting factor for the powder amorphization was the nucleation of the disordered TiAl intermetallic compound at an aluminium content of 60 at %, while a proposed thermodynamic model foresaw, for the Ti–Al system, a compositional range of amorphization up to an aluminium content of about 75 at % [6].

The attainment of Ti–Al powder batches with a chemical composition approaching the γ-TiAl phase, being either in the amorphous state or retaining a disordered fcc structure, may be promising for improvement of the mechanical properties of this intermetallic compound.

Recent studies on the modelling of the high-energy ball milling of elemental powders have pointed out that there is a strict dependence between the formation of an amorphous or a crystalline intermetallic

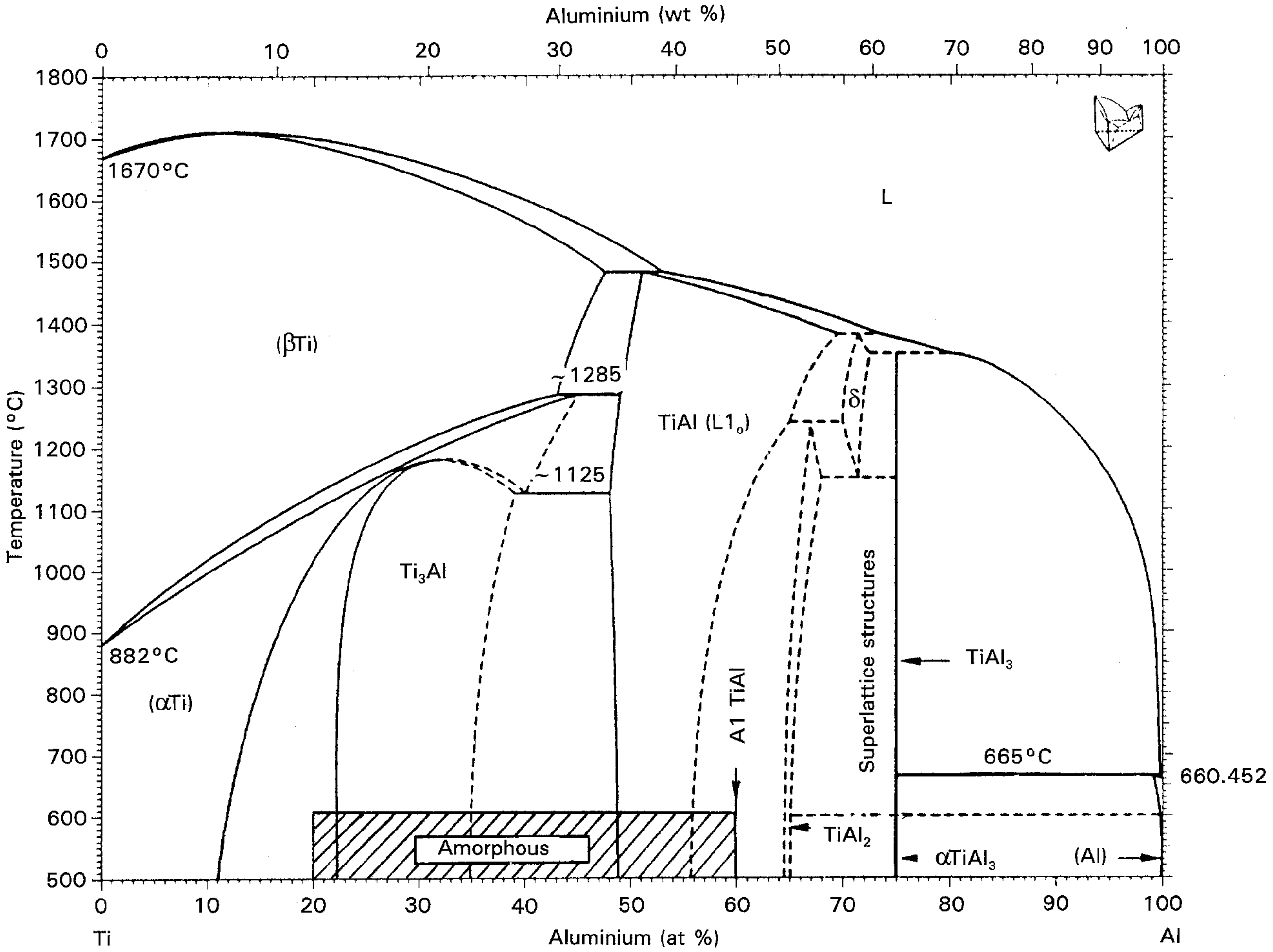

Figure 1 Equilibrium phase diagram of the Ti–Al system (reprinted from [14]). The dashed area indicates only the composition range of amorphous $Ti_{(1-x)}Al_x$ alloy prepared by MA.

phase and the applied milling conditions. More precisely, the amount of energy transferred to the powders during MA has been identified as a critical process variable [7, 8,]. It is, therefore, of some interest to examine, in more detail, the progress of the mechanical alloying process for aluminium-rich elemental powder mixtures focusing the attention on the mechanically driven SSR in connection with the applied milling conditions.

To these aims, several $Ti_{40}Al_{60}$ powder samples have been milled in a planetary mill under controlled energy-transfer conditions according to the description of the basic mechanics of the powder–workpiece interaction proposed for this kind of milling device [7]. Particular attention has been paid to avoid ambient gases contamination, because the ready solubility of oxygen and nitrogen into α-titanium and the continuous generation of rough and atomically clean surfaces during ball milling may substantially modify the process outcome [9, 10, 11].

2. Experimental procedure

2.1. Ball-milling procedure

Pure titanium (99.0%, 325 mesh) and aluminium (99.3%, 300 mesh, Alpha products) were used as starting powders. Because the titanium powder contained some amount of titanium hydride, due to the preparation method itself, it was previously submitted to a dehydrogenating treatment by vacuum annealing at intermediate temperature ($T = 800\,°C$).

Mechanical alloying was carried out in a Frisch-Pulverisette 5 planetary mill with hardened steel vials and balls. The ball-to-powder ratio was approximately 10:1. In order to minimize oxygen and nitrogen contamination, the vials were sealed under pure argon (1.5 atm), and all the operations which required opening the vials, for instance, loading or powder sampling, were performed inside a controlled argon atmosphere box ($O_2 < 3$ p.p.m., $H_2O < 5$ p.p.m.). To avoid an excessive warming up during milling, the vials were cooled by a forced air flow, and a cooling period of 30 min was interposed to equal milling time. Small quantities of powder were periodically withdrawn from the vials for X-ray diffraction analysis. At each sampling time, some milling balls were carefully weighed to measure the amount of powder coated on the ball surface to determine the quantity of powder involved during each ball impact.

The different milling conditions were obtained by loading the vials with balls of three different diameters ($\phi_b = 5$, 8 and 12 mm), while all the other parameters were kept constant.

2.2. X-ray diffraction analysis

X-ray diffraction patterns were recorded by computer-controlled Seifert PAD-VI and Siemens D-500 diffractometers in reflection geometry using MoK_{α} and Cu$K_{\alpha 1}$ (Johanson's Ge-monochromator) radiations ($\lambda = 0.07107, 0.15404$ nm), respectively. The recorded intensities were corrected for usual angular-dependent factors such as Lorentz and polarization effects. After correction the diffraction patterns were rescaled in wave number $h = 4\pi \sin\theta/\lambda$ (nm^{-1}) unit. To determine more precisely the angular position, integrated intensity and integral width of the reflection peaks, which showed, owing to the milling action, a growing broadening and overlapping, the corrected scattering curves were fitted by means of an ensemble of analytical profiles of the general type

$$f(h) = A[1 + B(h - h_r)^2]^{-C} \quad 1 < C < \infty \qquad (1)$$

where $h = 4\pi \sin\theta/\lambda$ is the angular variable, A is the intensity of the peak maximum, B is the half width of the reflection at half intensity, $h_r = 4\pi \sin\theta_r/\lambda$ is the centre angular position of the peak, and C is an exponent determining the profile shape ($C = 1$ Lorentzian profile, $C = \infty$ Gaussian profile).

The parameters A, B, h_r and C were optimized by a computer program [12]. The correction for instrumental broadening was not necessary in this instance. The integral width of a diffraction peak originated by the (hkl) family of the plane can be expressed as [13]

$$\delta h_{(hkl)}/2\pi = \alpha_{(hkl)}(h/2\pi) + 1/D_{(hkl)} \qquad (2)$$

where $\delta h/2\pi$ is the integral width of the (hkl) reflection, D is the mean grain size in the (hkl) direction, α is a constant related to lattice defects. The mean grain size of the crystallines in the (hkl) direction can be determined by extrapolating the integral width of two reflections, belonging to same family of planes, at $h = 0$.

According to Vujic *et al.* [2] the long-range order (LRO) parameter for the off-stoichiometric TiAl compound is defined as

$$S_{\mathrm{Ti}} = (r_{\mathrm{Ti}} - R_{\mathrm{Ti}})/(1 - R_{\mathrm{Ti}}) \qquad (3)$$

where r_{Ti} and R_{Ti} are the fraction of titanium atoms at titanium sublattice sites and the fraction of titanium atoms in the alloys, respectively. The LRO-parameter was graphically determined by comparing the ratio of the recorded intensities for superlattice and fundamental reflections together with the theoretical values calculated for a perfect ordered alloy.

2.3. Thermal analysis and O_2, N_2 determination

The thermal analysis was carried out in a Perkin–Elmer DSC 7 and in a Netsch DTA 409 instruments under purified argon flow. The oxygen and nitrogen contents of the milled and thermally treated samples were measured with a Leco TC 136 gas analyser.

3. Results

3.1. O_2, N_2 contamination

In Table I, the measured oxygen and nitrogen contents relative to the currently milled samples are reported. It can be noticed that some amount of oxygen and nitrogen is already present in the starting powder, but the contamination level does not grow appreciably at least during the first 30 h processing. The Ti–O and Ti–N phase diagrams [14] as well as the phase diagrams of the combined, substitutional and interstitial, Ti–Al–O and Ti–Al–N solid solution [15], indicate that the measured oxygen and nitrogen concentration should only cause a widening of the $(\alpha + \beta)$ region and a temperature rise of the titanium $\alpha \rightleftharpoons \beta$ allotropic transformation. Therefore, the effect of the contaminating gases can be reasonably neglected for the present purposes.

3.2. Mechanically induced SSR path

In Fig. 2a–c the X-ray diffraction patterns of the $Ti_{40}Al_{60}$ composition milled with balls of diameter $\phi_b = 5$, 8 and 12 mm are plotted as a function of the milling time. Two distinct SSR paths can be discerned.

Mechanical alloying performed with balls 5 and 8 mm in diameter (Fig. 2a and b) promotes the amorphization of the powders. The scattering curves attest the progressive vanishment of the crystalline diffraction peaks and the rise of a broad maximum. The position of this broad maximum lies at 27.35 nm^{-1}. The nearest neighbour distance of

TABLE I Oxygen and nitrogen contents measured on the starting materials, and on the milled or thermally treated $Ti_{40}Al_{60}$ samples

Nominal composition	O_2		N_2		Real composition	Ball diam. (mm)	Situation
	wt %	at %	wt %	at %			
Ti (as-received)	1.7	4.9	–	–	$Ti_{95.1}O_{4.9}$		
Ti (purged)	1.8	5.2	0.8	2.7	$Ti_{92.1}O_{5.2}N_{2.7}$		H-purging at 800 °C
Al	0.24	0.40	–	–	$Al_{99.6}O_{0.4}$		
$Ti_{40}Al_{60}$	1.03	2.20	–	–	$Ti_{39.1}Al_{58.7}O_{2.2}$		MA 0 h
	1.16	2.51	0.50	1.23	$Ti_{38.5}Al_{57.8}O_{2.5}N_{1.2}$	5	MA 5 h
	1.36	2.94	0.41	1.01	$Ti_{38.4}Al_{57.7}O_{2.9}N_{1.0}$	8	MA 5 h
	1.21	2.62	0.55	1.36	$Ti_{38.4}Al_{57.6}O_{2.6}N_{1.4}$	12	MA 5 h
	1.96	4.15	1.26	3.04	$Ti_{37.1}Al_{55.7}O_{4.2}N_{3.0}$	5	MA 30 h + TT 900 °C
	3.28	6.66	3.21	7.44	$Ti_{34.4}Al_{51.5}O_{6.7}N_{7.4}$	12	MA 70 h

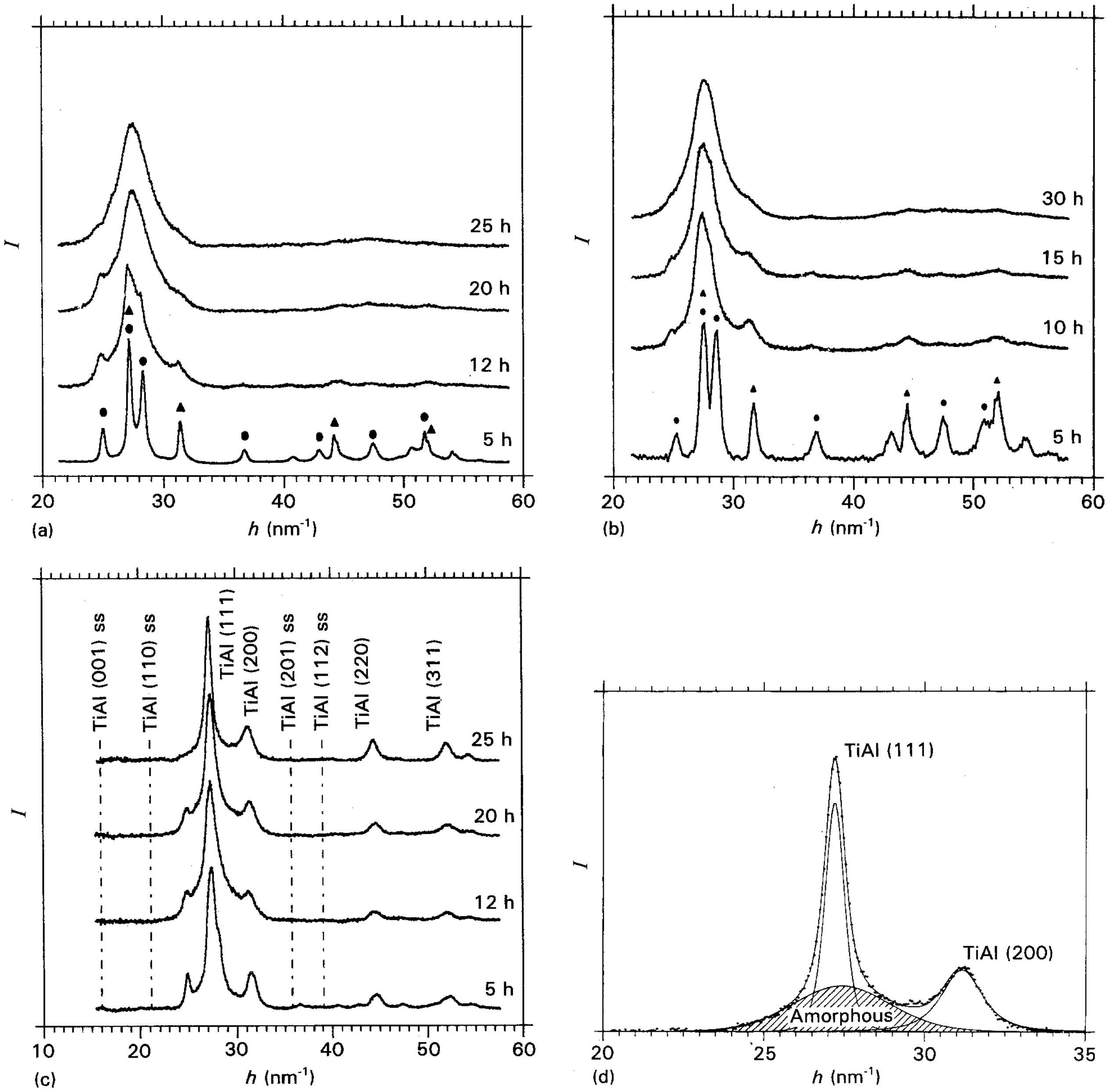

Figure 2 X-ray diffraction patterns of the mechanically alloyed samples plotted as a function of the milling time ($\lambda = \mathrm{Mo}K_\alpha$). Ball diameter, ϕ_b (a) 5, (b) 8, (c) 12 mm (the positions of the absent superlattice reflections are marked by ss); (d) X-ray spectrum with the Lorentzian peak components obtained by the fitting procedure for the powder after 25 h MA with $\phi_b = 12$ mm. The shadowed area shows the formation of an amorphous phase. (●) Ti(Al), (▲) Al.

0.28 nm agrees, in the Ehrenfest approximation [13], with the weighted sum of atom radii of aluminium and titanium.

In the case with balls $\phi_b = 12$ mm (Fig. 2c), the MA process cannot compel the powders to amorphize completely. The X-ray diffraction pattern after 25 h shows the formation of a simple crystalline structure superimposed on a partial amorphization of the powder (Fig. 2d). The diffraction lines can be indexed as the fundamental interference peaks of the $L1_0$–TiAl intermetallic compound (JCPDS n. 5-678). The only occurrence of all odd and even reflections indicates that the TiAl intermetallic holds an Al-fcc structure, without forming the layered $L1_0$-superlattice. The coexistence of an amorphous and a crystalline phase indicates that the two reaction paths are mutually competitive under this milling condition.

The diffraction patterns recorded after the early stage of alloying (Fig. 3a and b) point out that the mechanically driven SSR has already selected the two alternative reaction paths during the first 5 h processing. For the samples milled with ball of diameters $\phi_b = 5$ and 8 mm, MA causes a shift of the titanium-peaks towards higher scattering angle, i.e. a reduction in the lattice dimension. This peak shift is due to the diffusion of aluminium into titanium promoting the formation of α-Ti(Al) solid solution.

Milling with balls of diameter $\phi_b = 12$ mm promotes the nucleation of the Al-TiAl compound in concomitance with a less accentuated α-Ti peak displacement (Fig. 3c).

Table II gives the positions of the α-Ti(Al) (1 0 0) reflection for the samples milled for 5 h MA under the three different energy conditions. The corresponding

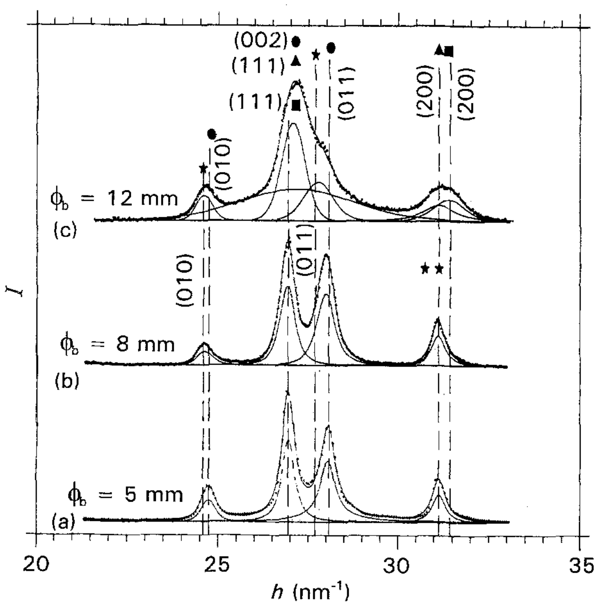

Figure 3 X-ray diffraction patterns of the sample milled under different energetic conditions after 5 h MA ($\lambda = \mathrm{Mo}K_\alpha$). The decomposition into single components shows the formation of a γ-Ti(Al) solid solution and the nucleation onset of the Al-TiAl intermetallic compound (●)α-Ti(Al); (▲)Al; (■)TiAl. The peak positions of pure Ti(∗) and Al(∗∗) are also indicated. The Ti(1 0 0) peak shift and the corresponding aluminium contents are reported in Table II.

TABLE II Lattice spacing of Ti(100) estimated by the fitting procedure for the $Ti_{40}Al_{60}$ powder after the early stage of ball milling (5 h). The corresponding aluminium content (at %) [16] is reported in the last column.

$h(\mathrm{nm}^{-1})$	Ti(010) d(nm)	 Δd(nm)	Solid solution Al (at %) [17]	Ball diameter (mm)
24.62^a	0.2552			
24.79	0.2535	− 0.0017	11.83	5
24.74	0.2540	− 0.0012	9.16	8
24.66	0.2548	− 0.0004	4.52	12

^a Pure titanium powder.

aluminium concentrations, calculated according to literature data [16] are also reported.

The surface-normalized quantity of powders ($\Delta m_S \mathrm{g\,m}^{-2}$) coated on the balls was measured through the difference in weight between a coated ball and a bare one: $\Delta m_S \approx 0.6 \pm 0.05 \times 10^{-2}\,\mathrm{g\,m}^{-2}$, for all three ball sizes.

3.3. Thermally induced SSR path on amorphous sample

To investigate a probable similarity of the energy given to the system either in the form of mechanical work or in the form of heat, the amorphous samples were submitted to differential scanning calorimetry analysis.

The measurements performed on the sample milled with balls of diameters $\phi_b = 5$ or 8 mm show the same results, so that only one set of measurements, with $\phi_b = 5$ mm, will be presented and discussed here.

Fig. 4 shows the differential scanning calorimetry (DSC) trace. The results of the thermogravimetric analysis (TGA) performed simultaneously, are plotted together. The DSC scan exhibits three main exothermic maxima associated with an irreversible transformation with a global heat release of about 9.4 kJ$(\mathrm{gat})^{-1}$. Because the TGA curve indicates no appreciable loss or increment of the powder weight during heating, the recorded heat release is not ascribable to oxidation or desorption phenomena. The X-ray diffraction pattern of the sample heated to 900 °C, during the DSC measurement, shows (Fig. 5b) that those several exothermic reactions end with the formation of the final stable α-TiAl compound. The

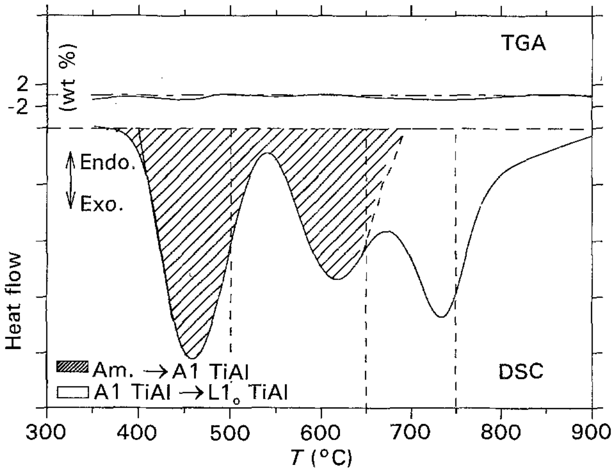

Figure 4 Differential scanning calorimetry (DCS) and thermogravimetric analysis (TGA) curves relative to the sample milled for 25 h with balls of diameter $\phi_b = 5$ mm. The shadowed areas indicate the distribution of the measured heat release between powder crystallization and ordering transition (see text). The temperatures of the additional heat treatments are indicated.

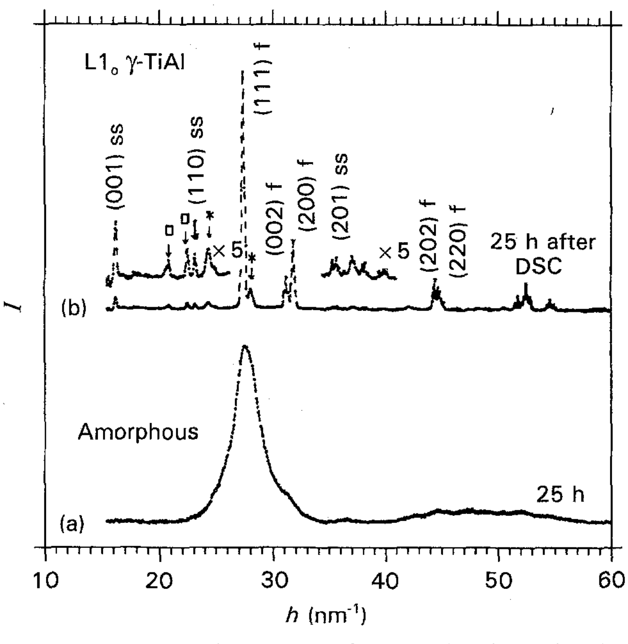

Figure 5 X-ray diffraction patterns of the samples after 25 h MA with balls of diameter $\phi_b = 5$ mm: (a) before DSC measurement; (b) after DSC ($T = 900\,°\mathrm{C}$). TiAl superlattice and fundamental reflections are marked by ss and f respectively, (∗) α-Ti(Al), (□) aluminium-rich component.

tetragonal superstructure of the equilibrium TiAl intermetallic compound is characterized by the superlattice peaks in the low-angle part of the diffraction pattern, as well as by the splitting of the (200) reflection. The lattice parameters of the unit cell, computed by least square refinement, are $a = 0.395$ nm and $c = 0.403$ nm ($c/a = 1.02$). The measured c/a axis ratio, which depends on the aluminium atomic percentage, corresponds to an aluminium concentration of about 50–55 at % [16]. The X-ray pattern also shows the presence of some additional low-intensity reflections, whose lattice spacings do not match any of the titanium, aluminium oxides and nitrides known from the literature. According to the results reported for rapidly quenched Ti–Al alloys [17], these diffraction lines could be indexed by the precipitation, inside the γ-(TiAl) matrix, of a titanium-rich solid solution isomorphous with α-titanium and of an aluminium-rich phase (JCPDS 18-0069, 26-0038).

To obtain further information on the structural changes during the entire DSC process, supplementary runs were performed at given temperatures of 500, 650 and 750 °C which correspond to the first two exothemic peaks at the DSC trace. The corresponding diffraction patterns are shown in Fig. 6.

A nearly identical situation can be gathered from the treatments at 500 and 650 °C. The amorphous structure is replaced by a crystalline phase. The X-ray diffraction pattern can be identified as the fcc structure of the disordered A1-form of the TiAl compound. However, the peak shape analysis (Fig. 6, insert) indicates that some amount of amorphous powder is still retained after thermal treatment at 500 °C.

The mean grain size along the (111) orientation, computed from the peak broadening (Fig. 7), does not show any difference: $D_{(111)} \approx 8$ nm for both cases. According to the X-ray diffraction results, the first two maxima in the DSC trace have been associated with the amorphous → A1-TiAl phase transformation with an enthalpy release of about 6.2 kJ $(\mathrm{g\,at})^{-1}$. Similar results have been also observed in another mechanically alloyed amorphous system [18], but no reasonable hypothesis can be drawn on the basis of the present results.

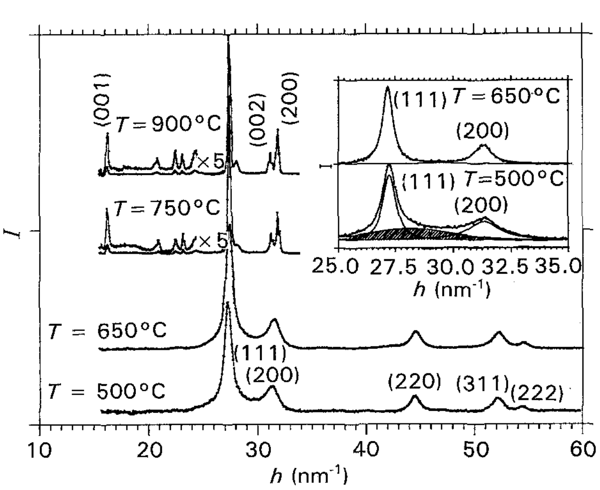

Figure 6 X-ray diffraction patterns of the MA samples (25 h) with balls of diameter $\phi_b = 5$ mm after different heat treatments. Insert: repetition in high-resolution conditions of the low-angle part of the patterns with heat treatment temperature of (a) 500 °C and (b) 650 °C ($\lambda = \mathrm{Cu}K_{\alpha 1}$). The peak shape analysis shows a retained amorphous component after heating up to 500 °C.

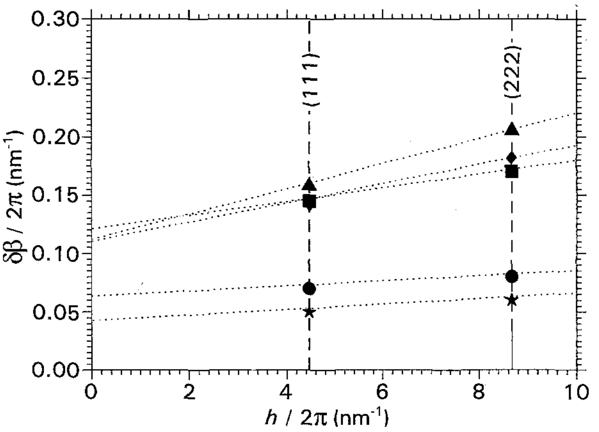

Figure 7 A plot of the integral width of the (1 1 1) and (2 2 2) reflections (belonging to the [1 1 1] family of plane) for various samples as a function of the exchanged vector module $h/2\pi = 2\sin\phi/\lambda$, at $h/2\pi = 0$, the integral width is expressed as $\delta h/2\pi = 1/D_{hkl}$, $(h\,k\,l) = (1\,1\,1)$ (see text). (■, ◆, ●, ★) $\phi_b = 5$ mm, (▲) $\phi_b = 12$ mm. T(°C): (■) 500, (◆) 650, (●) 750, (★) 900; (▲) MA 25 h.

The further treatments at higher temperatures ($T \geqslant 750$ °C) show, otherwise, the onset of the order transition indicated by the appearance of superlattice reflections and by the tetragonal distortion of the unit cell. Grain-size coarsening becomes appreciable at this temperature: $D_{(111)} \approx 16$–20 nm. Consequently, the last maximum corresponds to the irreversible ordering transition with an associated enthalpy release of 3.2 kJ $(\mathrm{g\,at})^{-1}$.

From the plot of the theoretical superlattice intensity ratio ($I_S/I_{(111)}$) versus long-range order parameter, [2], a long-range order parameter $S = 0.6 \pm 0.1$ can be derived for the $\mathrm{L1_0}$-TiAl sample after a thermal treatment at 900 °C for 2 h (Fig. 8).

4. Discussion

Eckert *et al.* [19] in their work have shown that, during the MA process, parent elements first deform into a multilayer agglomerate before any diffusional reaction might originate. The process of amorphization of elemental powders by MA has, therefore, often been assumed as analogous to the nucleation of amorphous phase during thermal annealing of layered composites. Because, in MA, the energy required to activate the solid-state reaction is mechanically supplied, the experimental feasibility of driving the induced SSR along two alternative paths, by simply changing the milling condition, underlines the need to examine the collision event in a greater details.

4.1. Modelling of ball impact

Ball impact is the basic mechanism by which energy can be transferred from the exterior to the powder particles. Neglecting sliding friction effects and assuming only front-head collisions to occur among balls

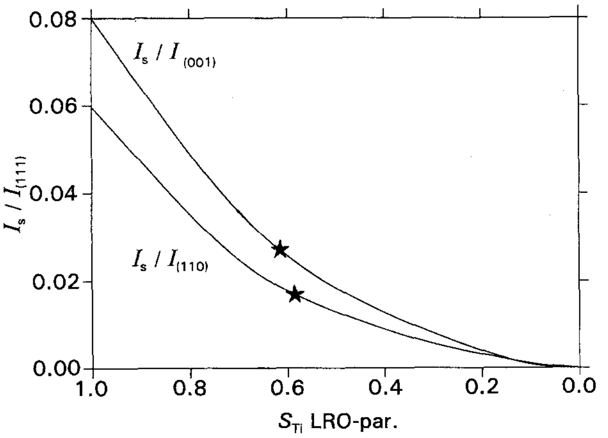

Figure 8 A plot of the theoretical superlattice intensity ratio $I_S/I_{(111)}$ versus long-range order LRO-parameter computed following Vujic *et al.* [2]. Experimental S value may be determined by superimposing experimental $I_S/I_{(111)}$ values (*) against the plot.

and vial, the amount of energy transferred from the milling media to the trapped powder during the collision, ΔE_r, can be expressed as

$$E_T(\text{J g}^{-1}) = KE_c/\Delta m_p \tag{4}$$

where E_c(J) is the kinetic energy of the colliding ball, Δm_p (g) is the mass of the trapped powder and K is a constant describing the kind of collision (K ranges between 0 and 1, 0 = elastic collision, 1 = inelastic collision). The kinetic energy of the colliding ball can be estimated from the equations describing its motion inside a milling vial [8]

$$E_c = \frac{1}{2} m_b v_b^2 \tag{5}$$

where v_b, the ball speed at the collision site, is equal to 3.2 m s^{-1} in the present case, m_b, the ball mass, is equal to 0.5, 2.1 and 7.1 g for the used sizes. The collision has proved to be inelastic during the early stage of MA, i.e. $K \approx 1$ [20].

Assuming that a layer of equal thickness will cover both the ball and the wall of the vial, the amount of trapped powder is

$$\Delta m_p = 2(\pi R^2 \Delta m_s) \tag{6}$$

where R is the Herzian radius of collision [21, 22], and Δm_s (g mm^{-2}) is the powder surface density.

TABLE III Calculated impact pressure, time and corresponding energy supply. (The impact pressure, p_{max}, and collision time, 2τ, are computed by the Herzian theory of collision [21, 22]: $p_{max}/E = 0.3521 v_b^{0.4} \ (\rho/E)^{0.2}$. Pa, $2\tau = 6.4034 v_b^{-0.2} \ (\rho/E)^{0.4} r_b$ s where E is the Young's modulus of the tools material (hardened steel: $E = 1.89 \times 10^{11}$), V_b is the ball impact velocity, m_b is the ball mass, r_b is the ball radius and ρ is the tool material density (7.8 g cm^{-3}.) The last column reports the powder adiabatic heating for the different milling conditions

Ball diameter ϕ_b (mm)	P_{max} (GPa)	2τ (10^{-5} s)	E_b (kJ mol^{-1})	Adiabatic heating (°C)
5	3.5	1.4	2.1	85
8	3.5	2.2	2.5	100
12	3.5	3.2	3.9	160

In Table III the computed values of the energy release during each collision are reported. The values are renormalized to J(g at)$^{-1}$. In the same table, other parameters, which can be calculated from the Hertz's theory of collision, such as impact duration time and pressure, are also indicated.

4.2. Milling condition versus induced SSR

The shortness of the collision time ($\approx 10^{-5}$ s) and the poor thermal conductivity W, of the material constituent the milling device (hardened steel, $W \approx 70$ J m^{-2} s^{-1}) allow us to consider the collision event as a quasi-adiabatic process. Thus, the energy released during one collision causes a momentary temperature rise of the trapped powder. According to the impact modelling, the temperature increase

$$\Delta T_{coll} = E_T/C_p \tag{7}$$

where C_p, the molar specific heat, is equal to about 25 J K^{-1}g^{-1}, reaches values of 85, 100 and 160 °C for balls of diameters $\phi_b = 5$, 8 and 12 mm, respectively. Meanwhile, ball milling also produces a considerable warming of the milling tools. In the present three cases, a average temperature of about 100 ± 20 °C inside the vial was experimentally measured after one milling period. Therefore, the actual temperature of deformed particles should range approximately between 200 and 300 °C.

On the other hand, the continuous defect generation is expected strongly to enhance atomic mobility [23, 24]. Eventually, the powder temperature rise and the diffusivity enhancement under plastic deformation may be regarded as the two main factors which control the kinetics of SSR induced by MA.

In spite of the formation of an energetically favoured equilibrium crystalline compound, the kinetics of phase formation may become the ruling factor owing to the low temperature at which the SSR takes place. Structurally simple phases, believed to have high nucleation rates and high growth velocities, may become a kinetically favoured pathway to lower the free energy of the system (maximum rate change of free energy $-\,\mathrm{d}(\Delta G)/\mathrm{d}t$ criterion) [25]. For instance, the formation of the amorphous phase ($\phi_b = 5$, 8 mm), which may be accomplished by just the movement of the faster atoms and a minor adjustment of the local position, could be expected to take place with a reaction time scale much smaller than the competitive crystalline equilibrium phase: $\delta t_a < \delta t_c$ (the subscripts represent amorphous TiAl and crystalline equilibrium phase, respectively.)

The equilibrium intermetallic compounds in the Ti–Al system are characterized by superstructure configurations: DO_{19}-Ti_3Al, $L1_0$-TiAl and $L1_2$-$TiAl_3$. A meaningful decrease of the interfacial energy can be achieved by the disordered metastable configuration of the intermetallic phase. As an example, the DO_{19}-Ti_3Al hexagonal superlattice transforms to A2-Ti_3Al, which is structually identical with the α-Ti(Al) terminal solid solution, whereas the disordered A1-TiAl, with its simplified f c c lattice, shows a close affinity to the structure of the parent material.

Considering the stable TiAl intermetallic, the nucleation of the A1 disordered form instead of the layered $L1_0$ structure does not presuppose a long-range ordering process with atomic exchange between neighbouring sites. It is reasonable to suppose that the formation of the A1-TiAl phase is kinetically favoured compared with the equilibrium one: $\delta t_d < \delta t_c$ (the subscript d represents the A1-fcc TiAl disordered compound). By increasing the energy transferred during each hit (ball diameter $\phi_b = 12$ mm), which means a higher temperature rise and higher strain level experienced by the powder, the nucleation rate of the A1-TiAl may become comparable with the amorphous one: $\delta t_d \approx \delta t_a < \delta t_c$, leading to the coexistence of amorphous phase together with the A1-TiAl compound.

4.3. Thermal analysis of amorphous samples

The DSC thermogram of Fig. 4 together with the diffraction patterns recorded at increasing temperatures (Figs 5 and 6) show clearly that the crystallization of the amorphous phase into the equilibrium γ-TiAl intermetallic compound follows two steps. As soon as the constituent atoms acquire a sufficient mobility ($T \approx 400\,°C$), the crystallization of the disordered A1-TiAl intermetallic phase is no longer hindered by the kinetic constraints. The self-diffusion coefficients for aluminium and titanium ($D_{Al} = 1.6 \times 10^{-11}\ cm^2\,s^{-1}$, $T = 400\,°C$; $D_{Ti} = 8.4 \times 10^{-14}\ cm^2\,s^{-1}$, $T = 700\,°C$ [26]) suggest, indirectly, the low mobility of titanium atoms to be responsible for the hindering of the ordering process at this intermediate temperature.

On increasing the temperature further, during the DSC scan, the titanium atoms may also diffuse. The mobility of both atomic species allows the system to overcome the energy barrier associated with the order transition and leads to the formation of the $L1_0$ fct. layered superstructure. The mobility of both type of atom is also confirmed by the sharpening of the diffraction lines associated with grain coarsening and lattice defect recovery.

It is of some interest to compare the estimated temperature reached by a powder particle at the collision instant under the high-energy milling condition ($\phi_b = 12$ mm), and the crystallization onset temperature of the amorphous powder ($T \approx 400\,°C$). In the first case, the assumption of a quasi-adiabatic process with ambient temperature rise inside the vial of about 100 °C yields an estimated temperature of the reacting interlayer $T \approx 300\,°C$. The approximation of these two temperature values may suggest a close affinity of the two processes. The different SSR paths observed by changing the milling conditions are probably related to the temperature rise of the trapped powder particles. This hypothesis is further confirmed by the fact that the only milled sample ($\phi_b = 12$ mm) and thermally treated ones have nearly equal crystalline dimensions (Fig. 6).

To our knowledge, the transition $A1 \rightarrow L1_0$ transition in the TiAl intermetallic compounds has never been experimentally observed before, only comparison with theoretical predictions is available.

Yang and Li [27], in the quasi-chemical approach, have found for the latent heat, ΔH_{d-o}, of the $A1 \rightarrow L1_0$ transformation, the following expression

$$\Delta H_{d-o} = -0.312\,RT_c \qquad (8)$$

where R is the gas constant ($R = 8.3169\ J\,mol^{-1}\,K^{-1}$) and T_c(K) the temperature above which the long-range order vanishes. Inserting for T_c the melting temperature of the TiAl compound ($T_c = T_m = 1723$ K) one obtains for a mole of TiAl compound: $\Delta H_{d-o} \approx -4.5\ kJ\,(g\,at)^{-1}$.

In a more recent "first principles" calculation [28] on the ordering energy of the TiAl compound, a value of $\Delta H_{d-o} \approx -17\ kJ\,(g\,at)^{-1}$ has been found as the difference between the formation energy of an ordered structure and the random alloy.

The measured enthalpy release, $\Delta H_{exp} \approx -3.2\ kJ\,(g\,at)^{-1}$ strongly departs from the theoretical predictions. The measured value of the degree of order $S = 0.6$, as well as the presence of short-range order in the A1 phase, may account for the low value of the released heat. Probably neither the distribution of the atomic species within each lattice site is completely random in the A1-TiAl compound nor the heat-treated powder corresponds to a perfectly ordered $L1_0$-TiAl intermetallic phase.

5. Conclusions

From the analysis of the present results on MA of the $Ti_{40}Al_{60}$ mixture under controlled milling conditions, the following conclusion can be drawn.

1. MA leads to the formation of an amorphous phase or to the nucleation of the A1-fcc non-equilibrium intermetallic compound by a proper choice of the milling conditions.
2. The compositional range of amorphization has been extended, on the aluminium-rich side, up to an aluminium concentration of 60 at %. The difficulty in nucleating the crystalline phase, postulated as a key criterion for solid-state amorphization, is dependent on the milling conditions.
3. Different milling conditions, i.e. different kinetic energy amounts of the milling balls, can be easily achieved by only changing the mass of the balls.
4. The total energy released to the unit of mass during each impact, assumed as inelastic, was estimated to be about 2.1, 2.5 and $3.9\ kJ(g\,at)^{-1}$ for the three different milling conditions selected in the present work. The corresponding adiabatic heating of the powder particles spans between 85 and 160 °C.
5. The two observed reaction paths are mainly ascribed to the influence that powder heating and plastic deformation have on the atomic mobility and on the nucleation rate of the amorphous and crystalline phase.
6. Differential calorimetric analysis of the amorphous samples has shown that the amorphous to crystalline transition follows two reaction steps. Firstly, at a temperature of about 400 °C, the amorphous powder transforms into the disordered A1-fcc TiAl form

with a heat of crystallization $\Delta H_{\text{crys.}} \approx -6.2\,\text{kJ}(\text{g at})^{-1}$. Upon further heating, the system undergoes an ordering transition with a measured enthalpy release $\Delta H_{\text{d}-\text{o}} \approx -3.2\,\text{kJ}(\text{g at})^{-1}$ of TiAl compound.

References

1. C. SURYANARAYANA, F. H. FROES and R. G. ROWE, *Int. Mater. Rev.* **36** (1991) 85.
2. D. VUJIC, Z. LI and S. H. WHANG, *Metall. Trans.* **19A** (1988) 2445.
3. C. C. KOCH, *Mater. Sci. Technol.* **15** (1991) 194.
4. W. GUO, S. MARTELLI, N. BURGIO, M. MAGINI, F. PADELLA, E. PARADISO and I. SOLETTA, *J. Mater. Sci.* **26** (1990) 6190.
5. L. SCHULTZ, *Mater. Sci. Eng.* **97** (1988) 15.
6. G. COCCO, I. SOLETTA, L. BATTEZZATI, M. BARRICCO and S. ENZO, *Philos. Mag.* **B61** (1990) 473.
7. N. BURGIO, A. IASONNA, M. MAGINI, S. MARTELLI and F. PADELLA, *Nuovo Cimento* **13D** (1991) 459.
8. F. PADELLA, E. PARADISO, N. BURGIO, M. MAGINI, S. MARTELLI, W. GUO and A. IASONNA, *J. Less-Common Metals* **175** (1991) 79.
9. W. GUO, S. MARTELLI, F. PADELLA, M. MAGINI, N. BURGIO, E. PARADISO and U. FRANZONI, *Mater. Sci. Forum* **88–90** (1991) 139.
10. U. MIZUTANI and C. H. LEE, *J. Mater. Sci.* **25** (1990) 399.
11. A. CALKA, *Appl. Phys. Lett.* **59** (1991) 1568.
12. D. W. MARQUART, *J. Soc. Ind. Appl. Math.* **91** (1963) 431.
13. A. GUINIER, "Théorie et Technique de la Radiocristallographie" (Dunod, Paris, 1964).
14. T. B. MASSALSKY, "Binary Phase Diagrams" (ASM, 1986).
15. "Phase Diagrams of Titanium Alloys" S. G. GLAZUNOV (ed.), Israel Program for Scientific Translation (1965).
16. W. B. PEARSON, "Handbook of Lattice Spacings and structure of Metals" (Pergamon Press, Oxford, 1967).
17. T. TANAMURA, T. SUGAI and M. TANINO, *J. Mater. Sci.* **25** (1990) 27.
18. H. BAKKER and L. M. DI, *Mater. Sci. Forum* **88–90** (1992) 27.
19. J. ECKERT, L. SCHULTZ and K. URBAN, *J. Non-Cryst Solids* **130** (1991) 273.
20. M. MAGINI, *Mater. Sci. Forum* **88–90** (1992) 121.
21. D. R. MAURICE and T. H. COURTNEY, *Metall. Trans.* **21A** (1990) 289.
22. S. P. TIMOSHENKO and J. N. GOODIER, "Theory of Elasticity" (McGraw-Hill, New York, 1970).
23. A. R. YAVARY and P. J. DESRÉ, *Phys. Rev. Lett.* **65** (1990) 2571.
24. G. MAZZONE, A. MONTONE and M. VITTORI-ANTISARI, *ibid.* **65** (1990) 2019.
25. U. GÖSELE and K. N. TU, *J. Appl. Phys.* **66** (1989) 2619.
26. "Handbook of Chemistry & Physics", 47th Edn (1966–1967)
27. L. GUTTMAN, *Solid State Phys.* **3** (1956) 1.
28. M. ASTA, D. DE FONTAINE, M. VAN SCHILFGAARDE, M. SLUITER and M. METHFESSEL, *Phys. Rev.* **B46** (1992) 5055.

Received 5 January
and accepted 1 September 1993